

## Microwave-assisted synthesis of CdS-reduced graphene oxide composites for photocatalytic reduction of Cr(VI)

*Xinjuan Liu<sup>a</sup>, Likun Pan<sup>a,\*</sup>, Tian Lv<sup>a</sup>, Guang Zhu<sup>a</sup>, Zhuo Sun<sup>a</sup>, Changqing Sun<sup>b</sup>*

<sup>a</sup>Engineering Research Center for Nanophotonics & Advanced Instrument,  
Ministry of Education, Department of Physics, East China Normal University,  
Shanghai, China

\*lkpan@phy.ecnu.edu.cn

<sup>b</sup>School of Electrical and Electronic Engineering, Nanyang Technological University,  
Singapore 639798 Singapore

### Experimental Section

#### Characterization

The surface morphology, structure and composition of the samples were characterized by field-emission scanning electron microscopy (Hitachi S-4800), high-resolution transmission electron microscopy (HRTEM, JEOL-2010), atomic force microscopy (AFM, SPI 3800N), Fourier transform infrared spectroscopy (FTIR, NICOLET NEXUS 670), Raman spectroscopy (LABRAM HRUV-VISIBLE, resolution: 1 cm<sup>-1</sup>), X-ray diffraction spectroscopy (Holland Panalytical PRO PW3040/60) with Cu K $\alpha$  radiation (V=30 kV, I=25 mA), and energy dispersive X-ray spectroscopy (JEM-2100), respectively. The Brunauer-Emmett-Teller (BET) specific surface areas ( $S_{\text{BET}}$ ) and the porosity of the samples were evaluated on the basis of nitrogen

adsorption isotherms measured at 77 K using a BELSORP-max nitrogen adsorption apparatus (Japan Inc.). All the samples were degassed at 150 °C before nitrogen adsorption measurements. The BET surface area was determined using the adsorption data in the relative pressure ( $P/P_0$ ) range of 0.05-0.35. The desorption isotherm was used to determine the pore size distribution using the Barret-Joyner-Halender (BJH) method. The UV-vis absorption spectra were recorded using a Hitachi U-3900 UV-vis spectrophotometer.

### **Photocatalytic experiments**

The photocatalytic performance of the as-prepared samples was evaluated by photocatalytic reduction of Cr(VI) under visible light irradiation. The samples (1 g/l) were dispersed in 60 ml Cr(VI) solutions (10 mg/l) which were prepared by dissolving  $K_2Cr_2O_7$  into deionized water. The mixed suspensions were first magnetically stirred in the dark for 30 min to reach the adsorption-desorption equilibrium. Under stirring, the mixed suspensions were exposed to visible light irradiation produced by a 400 W metal halogen lamp with cut off filter ( $\lambda > 400$  nm). At certain time intervals, 2 ml of the mixed suspensions were extracted and centrifugated to remove the photocatalyst. The filtrates were analyzed by recording UV-vis spectra of Cr(VI) using a Hitachi U-3900 UV-vis spectrophotometer.

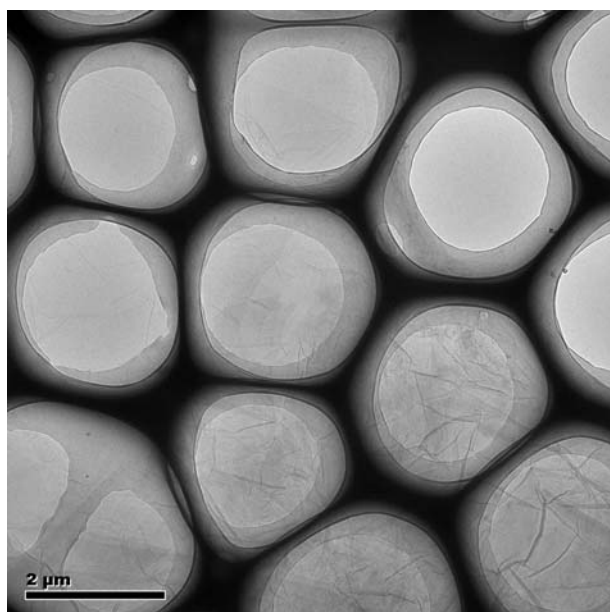


Fig. S1. HRTEM image of RGO.

Fig. S1 illustrates the HRTEM image of reduced graphene oxide (RGO). It is clearly observed that transparent ultrathin RGO with folds lay on copper grid.

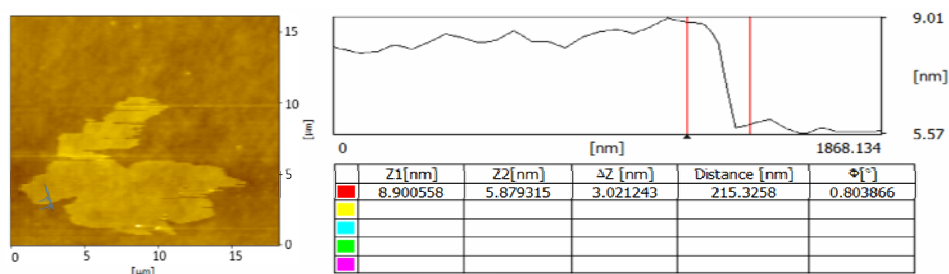


Fig. S2. AFM pattern of RGO.

Fig. S2 illustrates the AFM image of RGO. AFM was used to characterize the as-prepared RGO on a hydrophilic-treated silicon substrate by simple drop-casting of dilute RGO dispersion in ethanol solution. It can be observed from Fig. S2 that RGO sheet with large area is formed. Height profiles show the thickness of RGO is 3.0 nm, corresponding to the RGO of about three or four layers based on a theoretical value of

0.78 nm for single-layer graphene and the thickness contribution from oxygen-containing groups on the faces.<sup>1</sup>

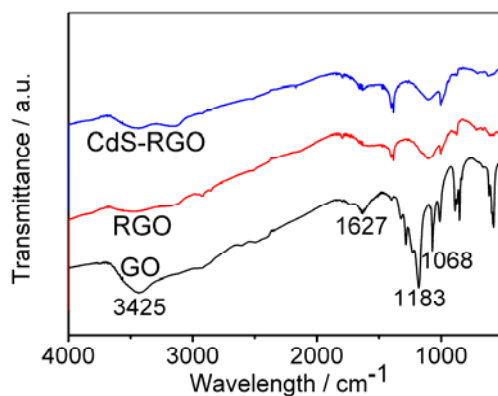


Fig. S3. FTIR spectra of GO, RGO, and CG-3.

Fig. S3 show the FTIR spectra of graphene oxide (GO), RGO, and CG-3. The broad absorption band at  $3425\text{ cm}^{-1}$  is assigned to the hydroxyl groups of adsorbed  $\text{H}_2\text{O}$  molecules. There is a obvious decrease in the intensities of  $\text{C}=\text{O}$  ( $1627\text{ cm}^{-1}$ ),  $\text{C}-\text{OH}$  ( $1183\text{ cm}^{-1}$ ) and  $\text{C}-\text{O}$  ( $1068\text{ cm}^{-1}$ ) stretching vibration peaks in RGO and CG-3 compared to those in GO, which suggests that microwave-assisted reduction is an effective method to remove oxygen-containing groups of GO.

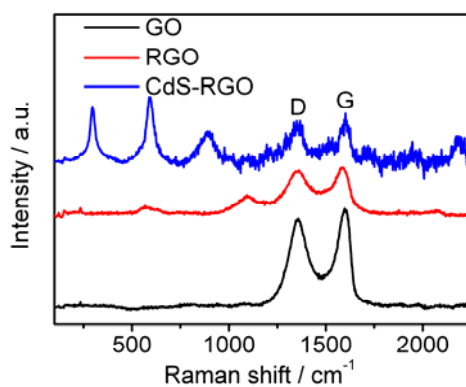


Fig. S4. Raman spectra of GO, RGO, and CG-3.

Fig. S4 display the Raman spectra of GO, RGO, and CG-3. The Raman spectrum of GO is dominated by two intensity peaks of carbon materials at 1354 and 1599  $\text{cm}^{-1}$ , which are referred as D band corresponding to the breathing mode of  $\kappa$ -point phonons of  $A_{1g}$  symmetry and G band assigned to the  $E_{2g}$  phonon of  $sp^2$  bonds of carbon atoms, respectively. For RGO nanosheets, the D band moves to 1348  $\text{cm}^{-1}$  and the G band shifts to 1585  $\text{cm}^{-1}$ , indicating the reduction of GO. For the CdS-RGO composite, all the Raman bands for CdS and RGO can be found. Two characteristic peaks of CdS at 295 and 591  $\text{cm}^{-1}$  correspond to the first and second-order LO phonon modes, respectively. Further, it is observed that RGO and CdS-RGO composite display an increased intensity ratio of the D peak and G peak ( $I_D/I_G$ ) in comparison to that of pure GO, showing a decrease in the average size of the  $sp^2$  domains upon the reduction of GO to RGO.<sup>2-4</sup> Similar trends are also observed in the transformation from  $\text{TiO}_2$ -GO to  $\text{TiO}_2$ -RGO composite.<sup>5,6</sup>

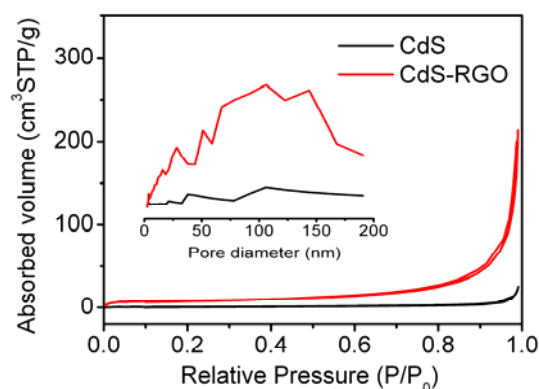


Fig. S5. Nitrogen adsorption-desorption isotherms and the corresponding pore size distribution curves (inset) of CdS and CG-3.

Fig. S5 displays the nitrogen sorption isotherms and the corresponding pore size distribution curves (inset in Fig. S5) for CdS and CG-3. The nitrogen sorption isotherms of CG-3 is similar to that of CdS and belongs to the type IV with a clear hysteresis loops, indicating the formation of mesoporous structures.<sup>4,7</sup> These isotherms exhibit H3 hysteresis loops associated with mesopores present in aggregates composed of primary particles, giving rise to slitlike pores. The pore size distributions (inset in Fig. S5) are very broad, indicating the existence of mesopores and macropores. From the adsorption branch of the isotherm curves, the BET specific surface areas of 2.5, 19.7, 25.5, 26.6, and 45 m<sup>2</sup> g<sup>-1</sup> are calculated for CdS, CG-1, CG-2, CG-3, and CG-4, respectively. It is reasonable to conclude that the BET specific surface area increases with the increasing RGO amount, which is beneficial for enhancing the photocatalytic activity.

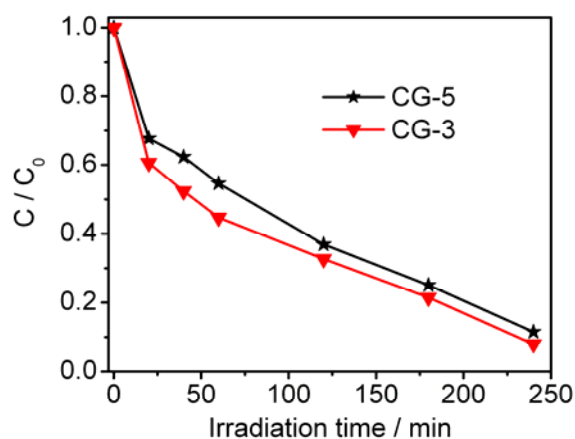


Fig. S6. Photocatalytic reduction of Cr(VI) by CG-3 and CG-5 under visible light irradiation. The concentrations of Cr(VI) and photocatalyst are 10 mg/L and 1 g/L, respectively.

Photocatalytic reduction of Cr(VI) by CG-3 and CG-5 was performed under visible light irradiation, as shown in Fig. S6. It is observed that higher photocatalytic performance of CG-3 is achieved via microwave-assisted method compared with CG-5 prepared using conventional solvothermal method. The higher photocatalytic performance of CG-3 should be ascribed to the following reasons: (i) Good contact between CdS and RGO is formed as a result of rapidly elevated temperature during microwave irradiation, which can inhibit the interfacial recombination of the injected electrons from CdS to RGO, leading to the enhancement of photocatalytic performance;<sup>8,9</sup> (ii) microwave irradiation can heat up the aqueous solution homogeneously and quickly because of the penetration characteristics of microwave and the high utilization factor of the microwave energy.<sup>10,11</sup> Therefore, the nucleation and growth of CdS can be finished in an extremely short period of time, which is extraordinarily beneficial for reducing the concentration of surface defects of CdS. The carrier recombination at surface defects of CdS is correspondingly suppressed, and thus the photocatalytic performance is increased.<sup>12,13</sup>

## References

- 1 H. B. Li, T. Lu, L. K. Pan, Y. P. Zhang and Z. Sun, *J. Mater. Chem.*, 2009, **19**, 6773.
- 2 K. F. Zhou, Y. H. Zhu, X. L. Yang, X. Jiang and C. Z. Li, *New J. Chem.*, 2011, **35**, 353.
- 3 Q. J. Xiang, J. G. Yu and M. Jaroniec, *J. Phys. Chem. C*, 2011, **115**, 7355.
- 4 Q. J. Xiang, J. G. Yu and M. Jaroniec, *Nanoscale*, 2011, **3**, 3670.
- 5 T. N. Lambert, C. A. Chavez, B. Hernandez-Sanchez, P. Lu, N. S. Bell, A. Ambrosini, T. Friedman, T. J. Boyle, D. R. Wheeler and D. L. Huber, *J. Phys. Chem. C*, 2009, **113**, 19812.

- 6 O. Akhavan, M. Abdolahad, A. Esfandiar and M. Mohatashamifar, *J. Phys. Chem. C*, 2010, **114**, 12955.
- 7 Q. Li, B. D. Guo, J. G. Yu, J. G. Ran, B. H. Zhang, H. J. Yan and J. R. Gong, *J. Am. Chem. Soc.*, 2011, **133**, 10878.
- 8 G. Zhu, L. K. Pan, T. Xu and Z. Sun, *ACS Appl. Mater. Interfaces*, 2011, **3**, 1472.
- 9 G. Zhu, L. K. Pan, T. Xu and Z. Sun, *ACS Appl. Mater. Interfaces*, 2011, **3**, 3146.
- 10 S. Komarneni, D. Li, B. Newalkar, H. Katsuki and A. S. Bhalla, *Langmuir*, 2002, **18**, 5959.
- 11 D. Chen, G. Shen, K. Tang, S. Lei, H. Zheng and Y. Qian, *J. Cryst. Growth*, 2004, **260**, 469.
- 12 L. J. Diguna, Q. Shen, J. Kobayashi and T. Toyoda, *Appl. Phys. Lett.*, 2007, **91**, 023116.
- 13 M. Shanmugam, M. F. Baroughi and D. Galipeau, *Thin Solid Films*, 2010, **518**, 2678.